A SPACECRAFT SIMULATOR FOR RESEARCH AND EDUCATION

ByungMoon Kim,[*] Efstathios Velenis,[†] Patrick Kriengsiri,[‡] and Panagiotis Tsiotras[§]

Georgia Institute of Technology
Atlanta, GA 30332-0150, USA

We present the details for the design and construction of a spacecraft simulator at the School of Aerospace Engineering of the Georgia Institute of Technology. The simulator is based on a hemi-spherical air bearing and its main purpose is the experimental validation of various spacecraft control strategies on the ground. Custom-made reaction wheels are used as torque actuators. The implementation of the attitude control algorithms is done on-board using a PC104 type Pentium 266MHz computer motherboard bundled with in-house software. We briefly discuss the major issues encountered during the design and construction of the simulator (such as sensor output filtering, motor parameters identification, etc) and the approaches developed to remedy these difficulties. To achieve a virtually torque-free environment it is necessary to carefully balance the spacecraft platform. We describe the method used to identify the moment of inertia of the platform and the center of gravity. Finally, we present some experimental results from the application of a simple LQR attitude stabilizing controller on the spacecraft simulator.

INTRODUCTION

It is envisioned that future commercial and military spacecraft will have an unprecedented degree of autonomy and pointing accuracy, made possible by increased on-board processing speed and memory capabilities. These on-board capabilities are imperative for the demanding tasks of future space missions, such as very-large base interferometry,[1–3] deployment of space optical telescopes, formation flying,[4–7] autonomous spacecraft docking, and servicing etc.[8–11] In the past several years, a plethora of spacecraft control techniques have been developed that address the challenging attitude tracking, stabilization and disturbance rejection requirements of these missions.

One major aspect that has been typically missing in the research area of attitude control development is the experimental validation of the theoretical results. Experimental testing is necessary before control laws can be incorporated in the future generation of spacecraft. The greatest difficulty in implementing spacecraft control laws is the fact that ground-based experiments must take place in a one-g environment, whereas the actual spacecraft will operate under zero-g conditions. Simulating a zero-g, torque-free environment is not an easy proposition. As a matter of fact, until recently only a few government laboratories [12,13] had the capability to experimentally validate attitude control laws in a realistic environment. With the recent explosion of commercial (as well as military) satellite industry there is an increased need for rapid prototyping and testing of the most promising attitude control algorithms proposed in the literature.

Several non-government agencies and academic institutions have recently initiated the development and construction of spacecraft simulators that can be used to educate the next generation of spacecraft dynamics

[*]Graduate Student, E-mail: gte342k@prism.gatech.edu, Tel: (404) 894-9108, Fax: (404) 894-2760.
[†]Graduate Student, E-mail: gte600q@prism.gatech.edu.
[‡]Undergraduate Student, E-mail: gte762i@prism.gatech.edu
[§]Associate Professor, E-mail: p.tsiotras@ae.gatech.edu, Tel: (404) 894-9526, Fax: (404) 894-2760. Corresponding author.

and control engineers. This article describes the recent efforts at the Georgia Institute of Technology to design, build and test such a (relatively low-cost) spacecraft simulator facility. The purpose of the GIT simulator is to evaluate and improve various theoretical controllers available in the literature, and to develop new control strategies in an experimental framework. This simulator is also used to demonstrate the fundamentals of spacecraft attitude dynamics, attitude estimation and control to the graduate and undergraduate students at Georgia Tech.

Accurate balancing of the platform is necessary to accurately duplicate a torque-free environment. Perfect balancing is obtained when the center of gravity coincides with the center of rotation of the platform. To achieve this goal, an identification algorithm was developed to estimate the moment of inertia matrix and the center of gravity of the whole platform. This algorithm can also be used to estimate the inertia matrix for later use in attitude tracking and indirect adaptive control schemes. The major components of the spacecraft simulator are described in detail in the sequel. Results from the testing of a linear stabilizing controllers are also reported.

OVERVIEW OF THE SPACECRAFT PLATFORM

The spacecraft "bus" at GIT consists of a 24in diameter (0.75in thick) aluminum disk that is supported on a hemi-spherical air bearing. The platform supports all the various spacecraft components, i.e., sensors, actuators, control computer, etc. See Fig. 1.

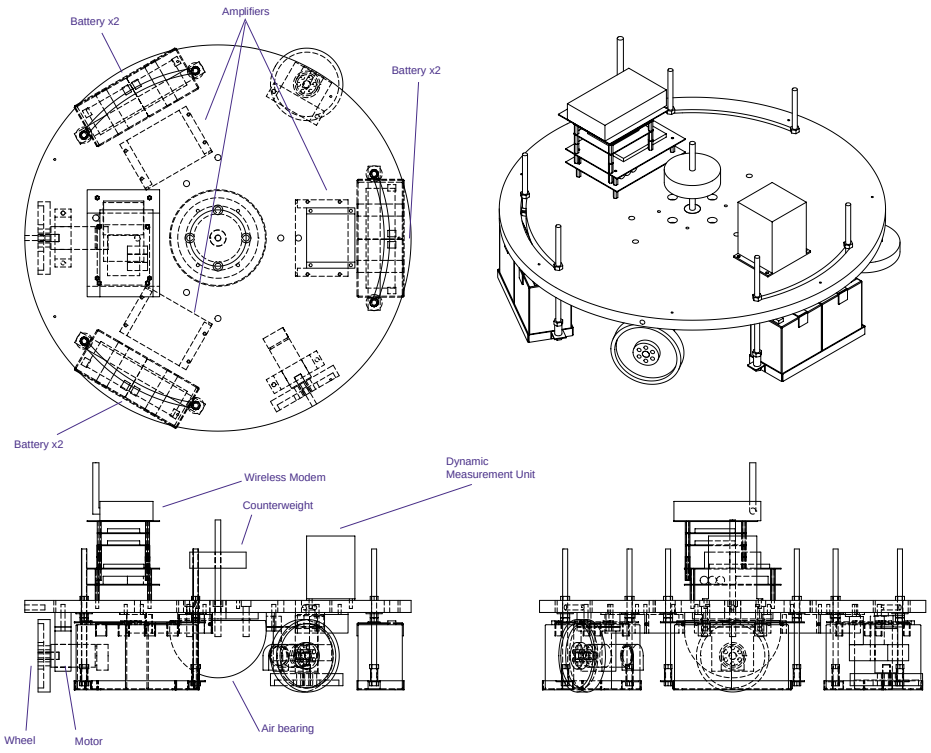

Figure 1: Schematic of spacecraft platform and components

The air-bearing is operated using compressed air from an external source through an air filter. The air filter removes moisture, oil and other impurities and regulates the air pressure (roughly around 25-40 psi depending on the normal load). Under the aluminum disk are mounted three wheels which can be operated at momentum or reaction wheel (RW) mode. The wheels are each paired with a DC motor and amplifier. Encoders installed on the DC motors provide angular feedback. Power for the entire system is provided by six 12V batteries connected pairwise in series to provide 24V at a time. On top of the aluminum disk, a

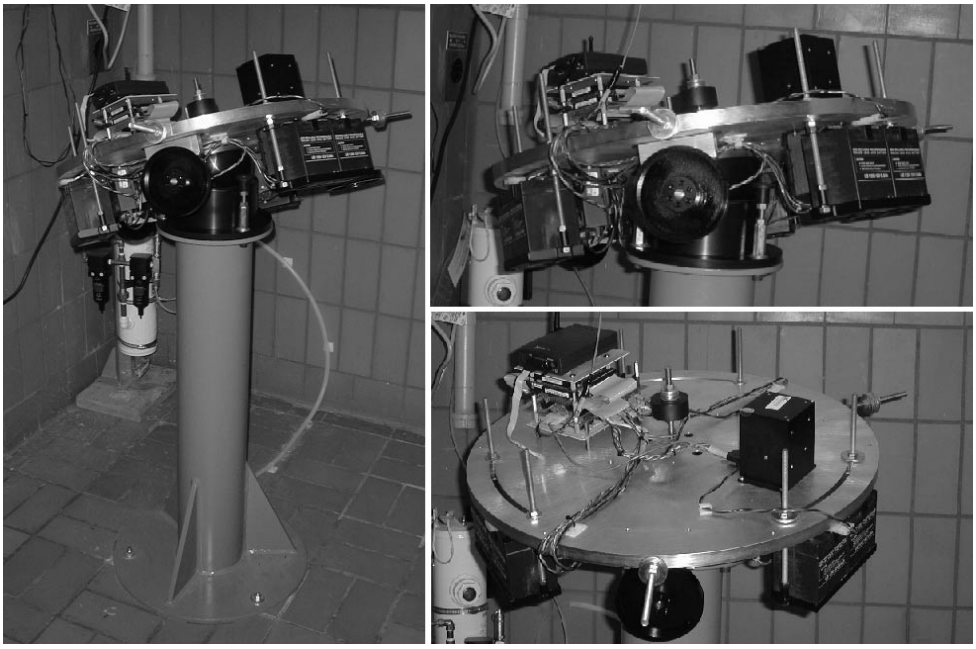

Figure 2: The Spacecraft Simulator.

PC104 type Pentium 266MHz main computer board (CMP5e) is used for the data acquisition, recording, controller implementation and communication. The remote PC and the CMP5e are connected via a wireless RS-232 serial port. The remote PC monitors the status of the experiments and issues control commands such as start/stop, while the CMP5e unit controls the motors directly.

In order to properly simulate the motion of a spacecraft in a gravity-free environment it is essential to balance the spacecraft platform so that the center of rotation coincides with its center of mass. Several counterweights are used to balance the whole assembly.

A photograph of the completed spacecraft simulator is shown in Fig. 2. An outline of the interconnection of the several simulator subsystems is shown in Fig. 3.

SUBSYSTEM DESCRIPTION

Air Bearing, Platform and Batteries

The air bearing that supports the platform is located on top of a pedestal structure (3 ft high) and it allows the platform to move without friction 30 deg about the two horizontal axes (x and y) and 360 deg about the vertical (z) axis. The bearing is the SRA 300 spherical air bearing designed and manufactured by Specialty Components Inc. The bearing itself is made of 6 00 aluminum and can hold up to 748 lbf of load when operating at 80 psi air pressure. The GIT platform bearing is operated at 30 psi which corresponds to approximately 300 lbf of vertical load.

The aluminum platform provides a mounting surface for the several simulator subsystems. The location of the center of mass (desired to be at the center of rotation of the simulator – in this case the center of the bearing rotor) can be changed by positioning different counterweights in various slots and holes located at several places on the platform. The platform was designed and manufactured in the Georgia Tech Aerospace machine shop. Care has been taken to position all major components of the simulator, such as momentum wheels, batteries, amplifiers, etc. in a symmetric fashion. This makes it easy to balance the platform as well as locate the principal axes.

Power to the simulator is provided by three pairs of rechargable Sealed Lead Acid batteries rated at 12 V

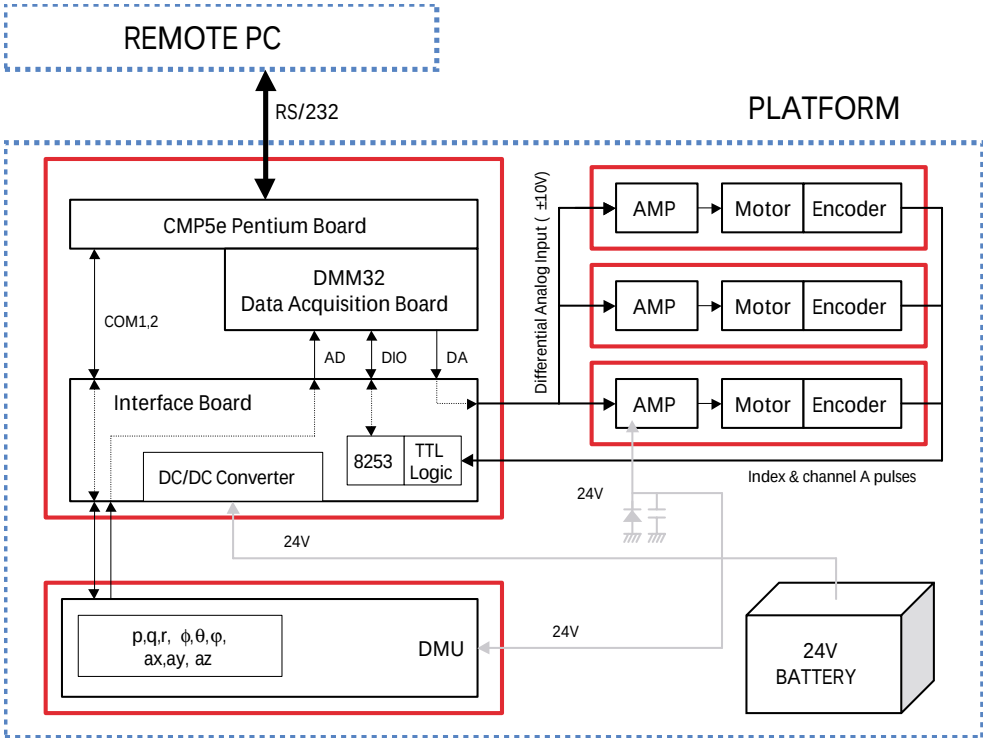

Figure 3: Overview of the spacecraft simulator component interconnection.

and 5 Ah. Each pair of batteries is connected in series to provide a 24 V. The batteries are then in turn connected to a DC converter which distributes the power to each spacecraft simulator component.

Spacecraft Attitude Sensor

The main purpose of the spacecraft simulator is to test several feedback attitude control laws. In order to implement the various controllers, measurements for the Eulerian angles and the angular rates is required. A dynamic measurement unit (DMU-AHRS) by Crossbow, Inc. was chosen as the attitude sensor unit. The DMU-AHRS provides Euler angles, angular rates, and linear acceleration. It can measure roll and pitch angles of $\pm$ 90° and heading angle of $\pm$ 180°. The RMS noise level in Euler angle measurement signal is 0.1°. The angular rate range is $\pm$ 150°/sec and the RMS noise level is 0.05°/sec. The accelerometer range is $\pm$ 2g and the RMS noise is 0.002g. Note that the peak to peak noise is about six times larger than the RMS noise level. All the measured values are available in both RS-232 and analog signal output. The analog signal provides faster sampling rates, while the RS-232 port provides digital data directly without introducing additional noise. The signals from the digital output were chosen after taking into account the requirements for noise-free operation.

Momentum Wheel Speed and Acceleration Sensor

Three encoders, rated at 500 counts/turn, are used to measure the angles of the momentum wheels. By differentiating these angles, the rotational velocities and accelerations of the wheels are calculated. A digital filter was designed to estimate angular velocities and accelerations from these angular position measurements. Alternatively, a tachometer can be used to measure angular velocity directly. Differentiation and filtering are still required to estimate angular acceleration in this case. We have used encoders instead of tachometers since the noise in the analog tachometer output can be avoided, and small velocities can be measured more accurately. One disadvantage of the encoders is that the time delay caused by filtering is typically larger than

that for the tachometer. This delay, however, can be kept small by careful filter design.

A flip/flop circuit was designed to get angular velocity and acceleration from the encoder signals. Specifically, each encoder has two slots, A and B, on its disk. These two slots provide two signals that have different phases, which give directional information. If A is in leading phase, the motor is spinning clockwise and vice versa. As is shown in Fig. 4, a flip-flop gate holds the status of A at the rising edge of B. When A is in leading phase, the flip-flop output, Q, is 1 and the counter 0 will have 500 pulses inputs per turn and vice versa. Thus, counters 0 and 1 measure clockwise and counter-clockwise rotation, respectively. The angle of the wheel is the difference between them. Figure 5 shows the complete schematic of the encoder signal pro-

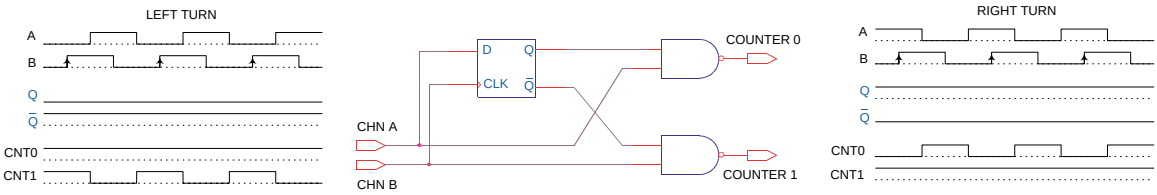

Figure 4: Encoder signal decoding

cessing circuits. Note that two 8253 timer/counters are used. Two 8253 have three counters each. Since three encoders need 6 counter, all counters in two 8253 were used. The control signals for the 8253 – i.e., address (A0,A1,A2), read (RD), write (WR), chip select (CS) and data signals (D0-D7) – are connected to the digital interface of DMM32. Thus, the control signals A0,A1,A2, RD, WR and CS are need to be implemented in software.

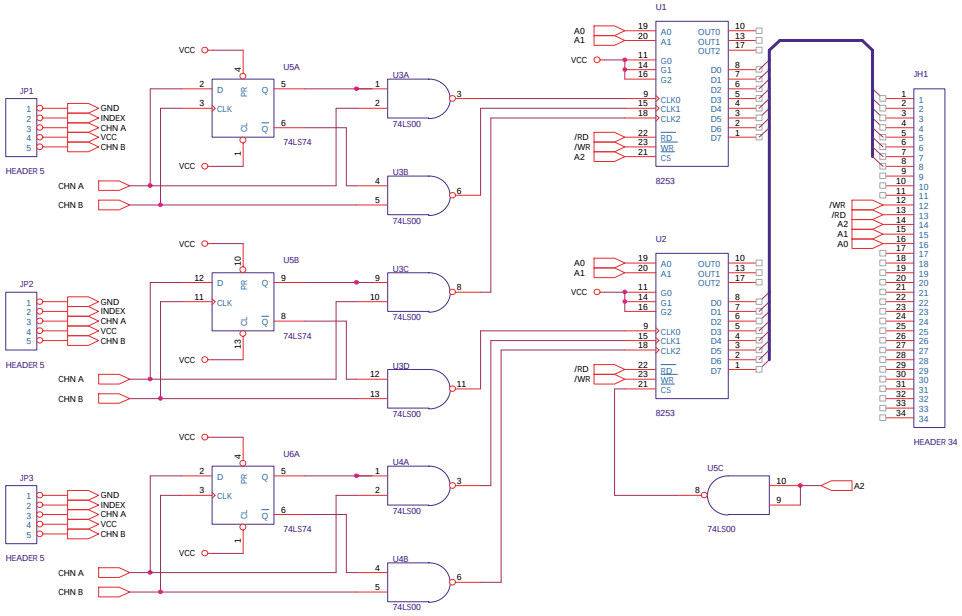

Figure 5: Encoder signal processing: phase detection and wheel turn count

Motors and Power Amplifiers

Three Maxon DC motors (Model 143683) with a 24V nominal voltage are used as actuators in lieu of expensive, space certified reaction/momentum wheels. The stall torque of each DC motor is 783mNm, the maximum continuous torque is 88.8mNm, and the maximum permissible speed is 8200rpm. Each motor is

driven by a Power Amplifier made by Copley Control (Model 403). It can deliver a continuous power of 120W (24V input) and peak power of 240W (24V input). The amplifier generates a PWM output for precise torque control. During initial testing, it was observed that this power amplifier produces reverse current in counter-clockwise spin, which can cause damage to the power supply circuit or other electronic components. Therefore, a diode (D1 in Fig. 6) was used to prevent the reverse current and a capacitor (C1 in Fig. 6) was used to flatten the power fluctuation. The power distribution schematic is shown in Fig. 6

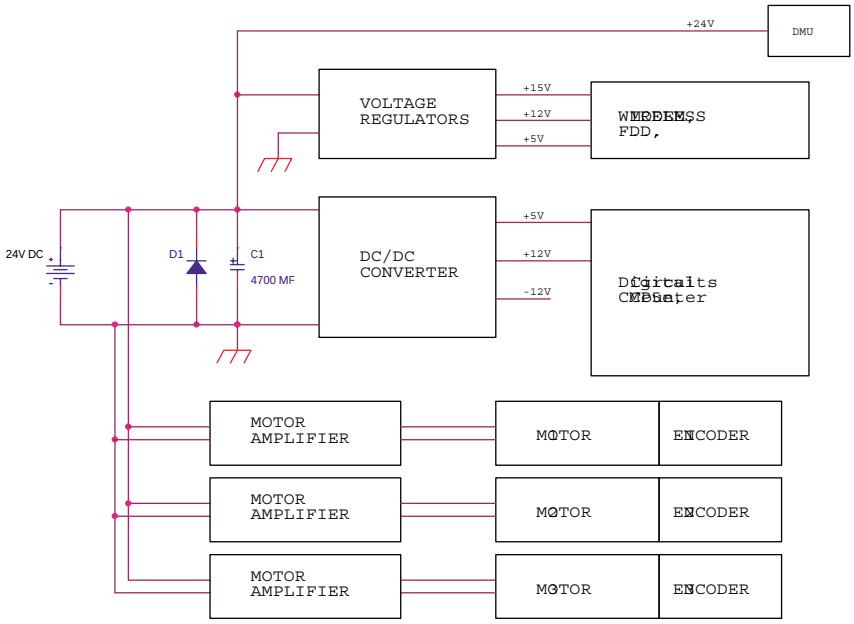

Figure 6: Power distribution diagram

The CPU and I/O Boards

The electronics suite includes the CPU unit, the I/O board, interface board and RF Modem; see Fig. 7. The CPU board runs the software that needs to handle all hardware controls, timers, packet-based communications, and filters for sensor signals. Although many of these tasks can even be done with a 8-bit CPU if the program is written carefully, fast 32bit processors are available in today's market at a reasonably low cost. We chose a PC104-type Intel mobile Pentium 266MHz board since various powerful software development tools and techniques for PC can be used without modification. The board model is CMP5e, from Ampro Computers. This CPU board has 32MB main memory, an 8MB memory disk and 2 Serial ports. The dimensions of the board are 3.6" x 3.8" x 0.9".

Three digital-to-analog converters are required for the motor amplifiers since they need analog inputs for the torque commands. The DMU needs 9 analog-to-digital converters for Euler angles, angular velocity and acceleration if analog outputs are used instead of digital outputs. Even if only digital outputs are chosen, A/D capability is still desired for future extension of the capabilities of the simulator. A digital interface is also required to read counter information. To meet all of these requirements, a PC104 type analog interface board, DMM32 (from Diamond Systems Corp.), is installed on top of the CMP5e. This board has 32 single-ended or 16 differential 16-bit A/D converters that have sampling rates of 200kHz, four 12-bit D/A converters and 24 programmable digital I/O. The CPU and I/O boards are shown in Fig. 8.

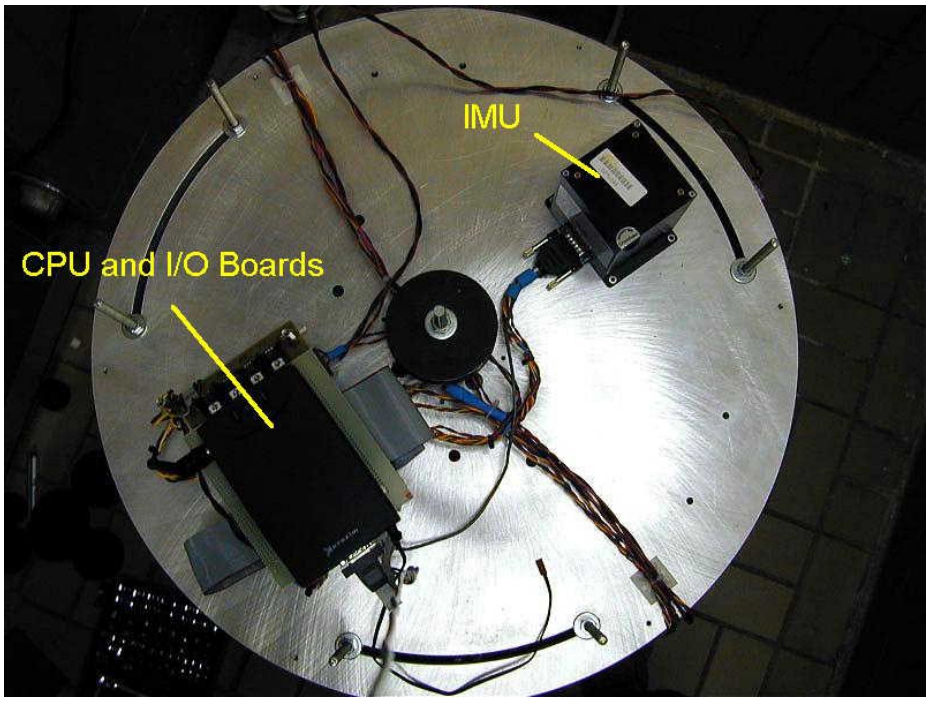

Figure 7: Top view of spacecraft platform

Interface Board

This board provides terminals for power, communications, as well as sensor signals for easy interface. Voltage regulators and a DC/DC converter for 5V, 12V and 15V voltage sources for various components are placed in this interface board. This board also has flip-flops and counters to measure the encoder signal. These counters are interfaced to the DMM32 via the digital I/O ports of the DMM32. The interface board was designed and built in-house.

Software

Two software applications were developed separately for both the CMP5e on-board computer and the remote PC computer. The latter is used to send initiate/stop commands, for health monitoring, post-experiment data analysis and plotting etc. The CMP5e and the remote host communicate via a wireless RF serial modem at a speed of 56K baud. The executable module for the CMP5e (`space.exe`) implements hardware initialization, controller initialization and starts a 0.1 millisecond precision timer to schedule various tasks and communications. This program is developed and compiled on the remote PC and then it is downloaded to the CMP5e via a serial communication interface. In cases `space.exe` has errors that cause the system to crash, the CMP5e needs to be restarted. When the CMP5e is restarted, a small starter program is then executed first and the onboard computer waits for a new executable of `space.exe` or a quit command. In the latter case, it executes the existing version of `space.exe`.

The remote PC runs a separate program (`ComCen.exe`). This is a multiple view-based GUI that implements the control toolbar, monitor view, message view and others. All multiple views are updated whenever a new data packet is delivered by a virtual `callback` function. The programs on the RemotePC and the onboard computer communicate with each other through an RS-232 serial connection with four types of custom developed packets: data, message, file and command packets. During the experiment, the time history of all state variables are recorded in a binary format history file. This file is transferred after the experiment to the remote PC and is converted to a `matlab *.m` file for further analysis.

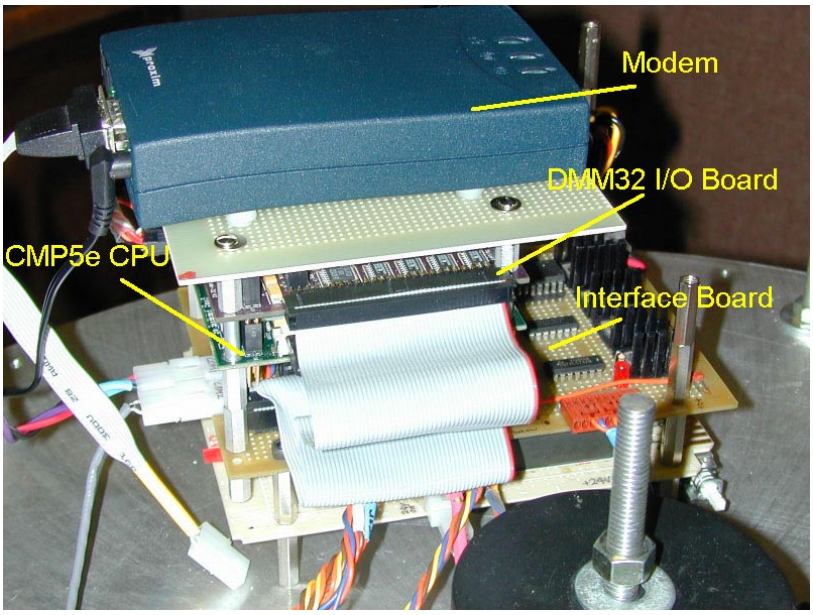

Figure 8: Close-up view of electronics

FILTERING AND IDENTIFICATION OF MOTOR PARAMETERS

Filter Design

Since the encoder signal provides angular information, we need to differentiate it once to get angular rate, and then once more to obtain angular acceleration, if necessary. Since differentiation of sensor signals always magnifies noise, filtering of the signal is necessary. For the spacecraft simulator, either a Butterworth or Chebyshev type 1 filter can be used, depending on the high frequency attenuation and time delay limitations. The frequency response of the filter used for angular rate and acceleration information is shown in Fig. 10.

Estimation of Motor Damping and Choice of Reaction Wheels

In order to keep the output torque sufficiently larger than the friction and magnetic damping torques, it is important to know the friction and magnetic damping effects of the motor. This allows proper sizing of the momentum wheels. In order to estimate the damping torque of the motor, the wheel was spun up to some high speed and then the motor/wheel was left to decelerate slowly due to those damping effects. Since the inertia of the wheel is accurately known, one can estimate the magnitude of the damping torque. Figure 11 shows the result of this experiment when the motor axis is horizontal. As is shown in this figure, the damping torque is increasing as the velocity increases and has a nonlinearity near zero velocity. Note that in the high-speed region, damping is not negligible and thus high-speed operation should be avoided. These damping torques can be an important factor that affects the sizing of the wheels. Larger wheels provide a larger torque and smaller damping. Smaller wheels provide good resolution in torque output but they also have more damping since they usually operate at higher speeds.

Identification of Motor Dynamics

The static motor gain can be calculated from the specifications of the motor, D/A converter setting and motor amplifier gain. However, by identifying the transfer function between torque command and response, we can calculate the dynamic behavior of the response as well as the gain of the motor. A least-squares fit was used for the transfer function identification. Figure 12 shows the transfer function between the voltage input to

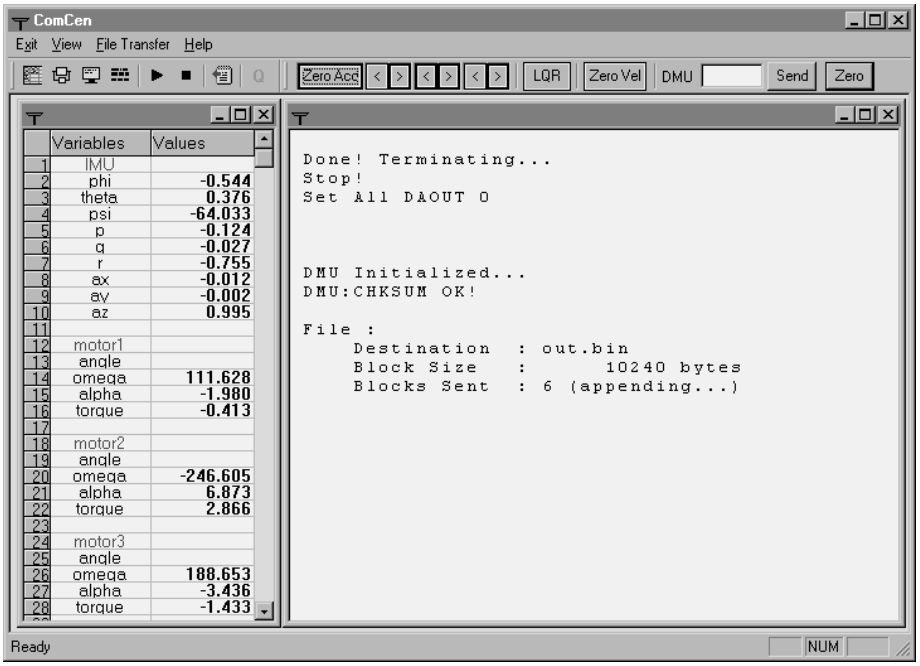

Figure 9: Remote PC side software panel

the amplifier and the torque output. The gain of the motor is about 0.4 Nm/Volt at zero frequency and it is decreasing at high frequency. As is shown in this figure, the motor response is quite fast and the gain does not change much up to approximately 10Hz. Since this frequency is much higher than the typical spacecraft torque response frequency, it was decided that additional efforts to improve motor response was not required.

IDENTIFICATION OF MOMENT OF INERTIA MATRIX

One way for calculating the moments of inertia is by using a CAD model. An AutoCAD model for the whole assembly was thus developed and mass densities for the various components were assigned for the whole system (see Fig. 1). This model was detailed enough to include small components such as bolts and nuts. The mass distribution of the sensor and electrical components were assumed to be homogeneous and the electrical

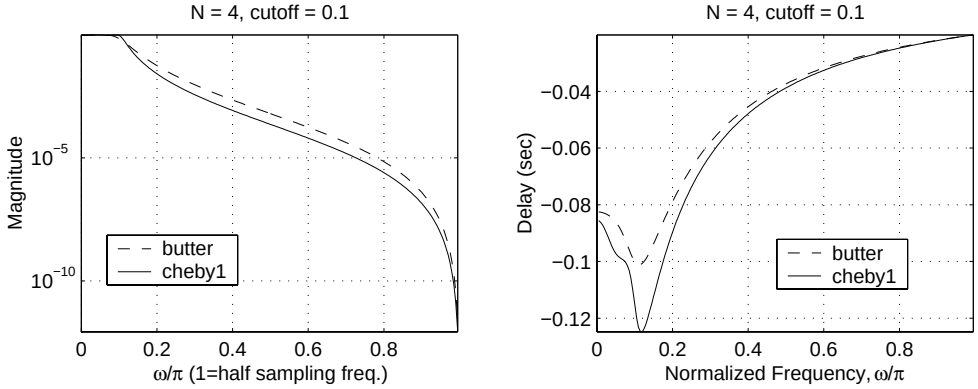

Figure 10: Filter design

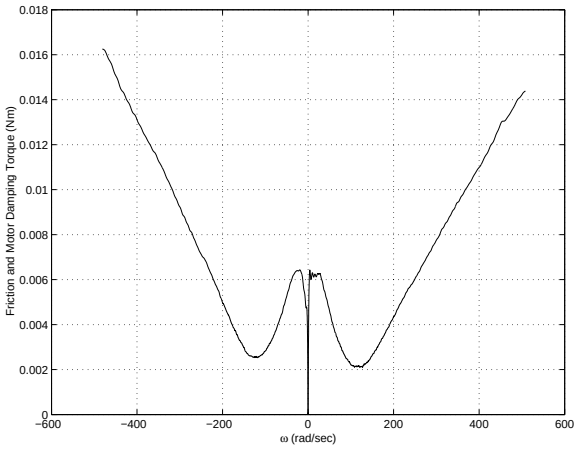

Figure 11: Friction torque versus speed during deceleration

wires and some other small electrical parts were neglected. This method gives a fairly accurate estimate of the inertia matrix with minimal effort. One drawback of the MOI estimation matrix using a technical drawing package such as AutoCAD is the difficulty associated with designing a complex 3D CAD model. On the other hand, experimental methods are not affected by the complexity of the structure. Traditional bifilar or trifilar pendulum methods can determine the inertia values from the period of the pendulum. Other experimental methods, such as the ones described in Refs. 14 and 15, measure the external reaction forces by load cells and find the inertia matrix that best fits the equation of motion in a least-squares sense. The major drawback of such methods is the significant amount of effort required for setting up and conducting the experiments.

Ideally, a spacecraft simulator operates in a torque-free (or almost torque-free) environment and there is no need to measure the reaction forces. Moreover, a spacecraft simulator has fully-featured motion sensors, which makes the experimental inertia estimation much simpler. In Ref. 16, the authors proposed the use of a coasting maneuver. A solution was found after converting the full nonlinear equation of motion to a standard least-squares form. An optimal coasting maneuver was also proposed based on stochastic analysis on the sensor noise. Another approach is realtime inertia estimation strategies for the case when the inertia of spacecraft is changing. Bergmann et al[17] proposed a mass property estimation strategy using nonlinear filtering, together with a simplified (nonlinear) model for the equation of motion. An input selection method to generate a feasible inertia estimation maneuver for this estimator was also proposed in Ref. 18. Other approaches for inertia estimation are those often found in spacecraft adaptive control literature. [19,20]

Below we describe the moment of inertia and center of gravity estimation scheme used for the GIT s/c simulator. The method is based on a standard least-squares identification algorithm using a series of experiments. In each experiment, a torque profile is commanded and the angular accelerations of the platform are recorded. Off-line analysis of the input-output data gives a very accurate estimation of both the moment of inertia matrix and the center of gravity of the platform. For the comparison purposes, the numerical approximation from AutoCAD model is also provided.

Representations of Attitude and Kinematics

A schematic of the spacecraft platform is shown in Fig. 13. Let an inertial frame I and a body frame S with their origins at the bearing center B^*, as in Fig. 13. The basis of I is denoted by $\vec{I},\vec{J},\vec{K}$ and the basis of S is denoted by $\vec{i},\vec{j},\vec{k}$. The unit vectors along the three wheel axes be denoted by $\vec{i}_{1,2,3}$. The unit vectors $\vec{i}_{1,2,3}$ are given in the body frame as

$$\vec{i}_1 = -\vec{i}, \qquad \vec{i}_2 = \frac{1}{2}\vec{i} + \frac{\sqrt{3}}{2}\vec{j}, \qquad \vec{i}_3 = \vec{k} \tag{1}$$

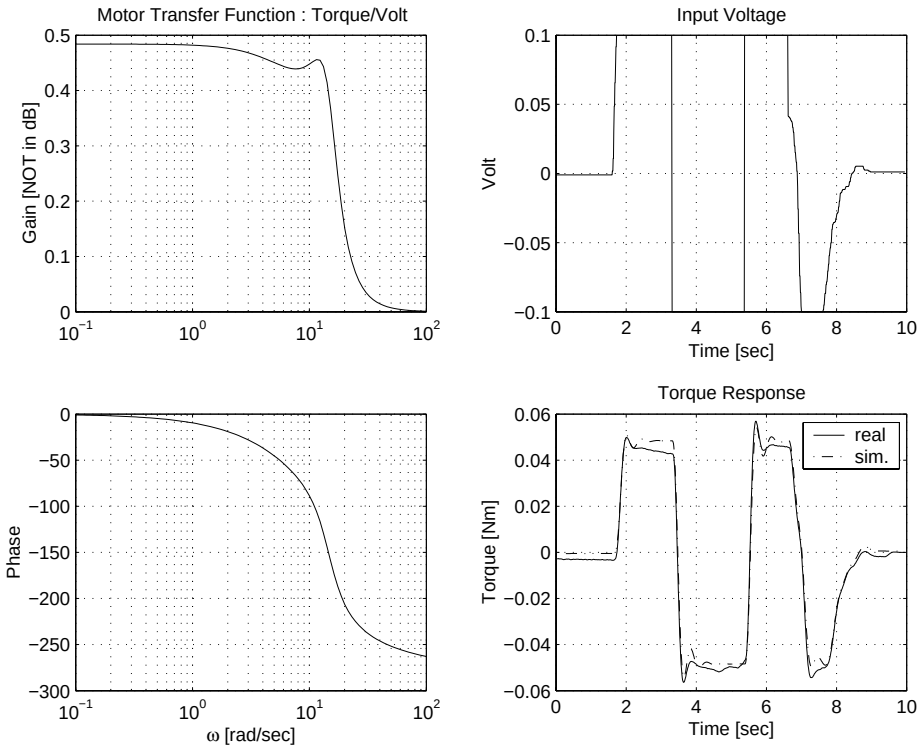

Figure 12: Identified motor dynamics and response comparison

To describe the attitude of spacecraft, a 3-2-1 Euler angle sequence. The relevant direction cosine matrix (DCM) that is used to represent the transformation from the inertial frame to the spacecraft body frame is given by

$$(2) \qquad [T]_{IS} = \begin{bmatrix} \vec{i}\cdot\vec{I} & \vec{i}\cdot\vec{J} & \vec{i}\cdot\vec{K} \\ \vec{j}\cdot\vec{I} & \vec{j}\cdot\vec{J} & \vec{j}\cdot\vec{K} \\ \vec{k}\cdot\vec{I} & \vec{k}\cdot\vec{J} & \vec{k}\cdot\vec{K} \end{bmatrix} = \begin{bmatrix} c_\theta c_\psi & c_\theta s_\psi & -s_\theta \\ s_\phi s_\theta c_\psi - c_\phi s_\psi & s_\phi s_\theta s_\psi + c_\phi c_\psi & s_\phi c_\theta \\ c_\phi s_\theta c_\psi + s_\phi s_\psi & c_\phi s_\theta s_\psi - s_\phi c_\psi & c_\phi c_\theta \end{bmatrix}$$

The kinematic equations are given by

$$(3) \qquad \begin{Bmatrix} \dot{\phi} \\ \dot{\theta} \\ \dot{\psi} \end{Bmatrix} = \begin{bmatrix} 1 & \sin\phi\tan\theta & \cos\phi\tan\theta \\ 0 & \cos\phi & -\sin\phi \\ 0 & \sin\phi/\cos\theta & \cos\phi/\cos\theta \end{bmatrix} \begin{Bmatrix} p \\ q \\ r \end{Bmatrix}$$

Equation of Motion

The full nonlinear equations of motion can be derived starting from the momentum of a differential mass element δm as illustrated in Fig. 14. Note that the center of mass is located at S^*. The velocity of δm is given by $\vec{v} = {}^I\vec{\omega}^S \times \vec{r}$ where $\vec{r}$ is the position vector from B^*. The velocity of a differential mass δm of the wheel is given by

$$(4) \qquad \vec{v}_{w_i} == {}^I\vec{\omega}^S \times \vec{r}_{w_i} + {}^S\vec{\omega}^{w_i} \times \vec{\rho}$$

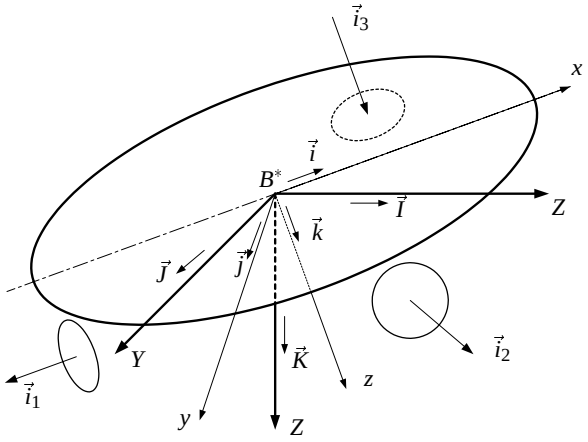

Figure 13: Definition of coordinates

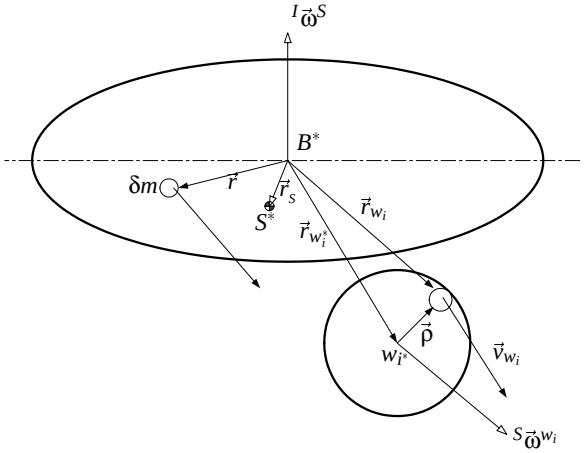

Figure 14: Definition of mass center and momentum of δm

The angular momentum of whole system is calculated as

$$
\begin{aligned}
\vec{H} &= \int_S \vec{r} \times \left({}^I\vec{\omega}^S \times \vec{r} \right) \delta m + \sum_{i=1}^{3} \int_{w_i} \vec{r}_{w_i} \times \left({}^I\vec{\omega}^S \times \vec{r}_{w_i} + {}^S\vec{\omega}^{w_i} \times \vec{\rho} \right) \delta m \\
&= \int_{S+w} \vec{r} \times \left({}^I\vec{\omega}^S \times \vec{r} \right) \delta m + \sum_{i=1}^{3} \int_{w_i} \vec{r}_{w_i} \times \left({}^S\vec{\omega}^{w_i} \times \vec{\rho} \right) \delta m \\
&= \underline{\underline{\mathbf{I}}}^{(S+w)/B^*} \, {}^I\vec{\omega}^S + \sum_{i=1}^{3} \vec{r}_{w_i^*} \times \left({}^S\vec{\omega}^{w_i} \times \int_{w_i} \vec{\rho} \, \delta m \right) + \sum_{i=1}^{3} \int_{w_i} \vec{\rho} \times \left({}^S\vec{\omega}^{w_i} \times \vec{\rho} \right) \delta m \\
&= \underline{\underline{\mathbf{I}}}^{(S+w)/B^*} \, {}^I\vec{\omega}^S + \underline{\underline{\mathbf{I}}}^{w_i/w_i^*} \, {}^S\vec{\omega}^{w_i}
\end{aligned}
\tag{5}
$$

where $\underline{\underline{\mathbf{I}}}^{w_i/w_i^*}$ is the inertia dyadic of i^{th} wheel with respect to the wheel's mass center w_i^*. $\underline{\underline{\mathbf{I}}}^{(S+w)/B^*}$ is the inertia dyadic for the eitire body of spacecraft and wheel with respect to bearing center $B*$. For convenience, let $\underline{\underline{\mathbf{I}}} \equiv \underline{\underline{\mathbf{I}}}^{(S+w)/B^*}$ and $\underline{\underline{\mathbf{I}}}^i \equiv \underline{\underline{\mathbf{I}}}^{w_i/w_i^*}$. Since viscosity effects of the air bearing are neglected and pressure is always normal to the spherical bearing surface, the only external torque exerted on the bearing center is the one by

gravity. Euler's theorem gives the equations of motion of the platform as

$$
\begin{aligned}
\vec{T} &= \vec{r}_S \times mg\vec{k} = (mg\,\vec{r}_S) \times \vec{k} \\
&= \frac{{}^S d}{dt}\left(\underline{\underline{\mathbf{I}}}^I \vec{\omega}^S\right) + {}^I\vec{\omega}^S \times \underline{\underline{\mathbf{I}}}^I \vec{\omega}^S + \sum_{i=1}^{3}\left(\frac{{}^{w_i} d}{dt}\left(\underline{\underline{\mathbf{I}}}^{i\,S}\vec{\omega}^{w_i}\right) + {}^I\vec{\omega}^{w_i} \times \underline{\underline{\mathbf{I}}}^{i\,S}\vec{\omega}^{w_i}\right) \\
&= \underline{\underline{\mathbf{I}}}^I \dot{\vec{\omega}}^S + {}^I\vec{\omega}^S \times \underline{\underline{\mathbf{I}}}^I \vec{\omega}^S + \sum_{i=1}^{3}\left(\underline{\underline{\mathbf{I}}}^{i\,S}\dot{\vec{\omega}}^{w_i} + \left({}^I\vec{\omega}^S + {}^S\vec{\omega}^{w_i}\right) \times \underline{\underline{\mathbf{I}}}^{i\,S}\vec{\omega}^{w_i}\right)
\end{aligned} \tag{6}
$$

Let a unit vector along the symmetry axis of the wheel w_i be $\vec{i}_i$ and choose the other two bases vectors $\vec{j}_i$ and $\vec{k}_i$ so that they are orthonormal and form right handed coordinate system. Since the wheels are axisymmetric, $\underline{\underline{\mathbf{I}}}^i = I_{11}^{w_i}\vec{i}_i\vec{i}_i + I_{22}^{w_i}\vec{j}_i\vec{j}_i + I_{33}^{w_i}\vec{k}_i\vec{k}_i$. Also, since the wheels always rotate along $\vec{i}_i$, ${}^S\vec{\omega}^{w_i} = \omega_i\vec{i}_i$. As a result,

$$
\begin{aligned}
{}^S\vec{\omega}^{w_i} \times \underline{\underline{\mathbf{I}}}^{i\,S}\vec{\omega}^{w_i} &= \omega_i\vec{i}_i \times \left(I_{11}^{w_i}\vec{i}_i\vec{i}_i + I_{22}^{w_i}\vec{j}_i\vec{j}_i + I_{33}^{w_i}\vec{k}_i\vec{k}_i\right) \cdot \omega_i\vec{i}_i \\
&= \omega_i\vec{i}_i \times \left(I_{11}^{w_i}\omega_i\vec{i}_i\right) \;=\; 0
\end{aligned} \tag{7}
$$

Finally, we have

$$
(mg\,\vec{r}_S) \times \vec{k} = \underline{\underline{\mathbf{I}}}^I \dot{\vec{\omega}}^S + {}^I\vec{\omega}^S \times \underline{\underline{\mathbf{I}}}^I \vec{\omega}^S + \sum_{i=1}^{3}\left(\underline{\underline{\mathbf{I}}}^{i\,S}\dot{\vec{\omega}}^{w_i} + {}^I\vec{\omega}^S \times \underline{\underline{\mathbf{I}}}^{i\,S}\vec{\omega}^{w_i}\right) \tag{8}
$$

Estimation of the Inertia Matrix

Since our experimental platform uses three momentum wheels, we can achieve arbitrary motion by sending acceleration commands to the wheels. Assuming that aerodynamic and motor bearing friction forces are small, the only external torque is the torque caused by gravity, which can be identified along with the inertia matrix. The estimation scheme uses the fact that the equations of motion are linear with respect to the inertia components and gravity. Thus, the estimation problem can be solved easily by a least-squares algorithm implemented in regression form.[16]

$$
[A]\{x\} = \{y\} \tag{9}
$$

During identification, wheel acceleration commands are applied in all three directions $\vec{i}, \vec{j}$ and $\vec{k}$ defined in Fig. 13. Since the platform cannot exceed pitch and roll ranges in excess of $\pm 30\,\text{deg}$, a stabilizing LQR controller is turned on to reorient the platform to the initial position if the angular pitch and roll motions exceed these values.

To derive the regression expression (9) from equation (8), we need to re-write the latter in matrix form. To this end, let T_{w_iS} be the transformation matrix from frame of i^{th} wheel $(\vec{i}_i, \vec{j}_i, \vec{k}_i)$ to S $(\vec{i}, \vec{j}, \vec{k})$. From Figure 15, T_{w_iS} are given as

$$
T_{w_1S} = \begin{bmatrix} -1 & 0 & 0 \\ 0 & -1 & 0 \\ 0 & 0 & 1 \end{bmatrix}, \quad T_{w_2S} = \begin{bmatrix} 1/2 & -\sqrt{3}/2 & 0 \\ \sqrt{3}/2 & 1/2 & 0 \\ 0 & 0 & 1 \end{bmatrix}, \quad T_{w_3S} = \begin{bmatrix} 0 & 0 & 1 \\ 0 & 1 & 0 \\ 1 & 0 & 0 \end{bmatrix} \tag{10}
$$

Let $\{\vec{\omega}\}_S$ and $[\underline{\underline{\mathbf{I}}}]_S$ be $\vec{\omega}$ and $\underline{\underline{\mathbf{I}}}$ written in frame S, respectively. Let $[\tilde{\omega}]_S$ denote the cross product in matrix form.[21] Using the fact that $\underline{\underline{\mathbf{I}}}^{i\,S}\vec{\omega}^{w_i} = I_{11}^{w_i}\omega_i\vec{i}_i$ and by defining $\{{}^I\vec{\omega}^S\}_S \equiv [p\;q\;r]^T$ one finally obtains

$$
\vec{T}_S = mg\{\vec{r}_S \times \vec{K}\}_S = -[\tilde{K}]_S\{mg\,\vec{r}_S\}_S \tag{11}
$$

where $\{\vec{K}\}_S$ is $\vec{K}$ expressed in the spacecraft body frame. Note that $\{\vec{K}\}_S$ is a function of ϕ, θ and ψ as follows

$$
\{\vec{K}\}_S = \begin{Bmatrix} \vec{i}\cdot\vec{K} \\ \vec{j}\cdot\vec{K} \\ \vec{k}\cdot\vec{K} \end{Bmatrix} = \begin{Bmatrix} 2(q_1q_3 + q_2q_4) \\ 2(q_2q_3 - q_1q_4) \\ -{q_1}^2 - {q_2}^2 + {q_3}^2 + {q_4}^2]^T \end{Bmatrix} = \begin{Bmatrix} -\sin\theta \\ \sin\phi\cos\theta \\ \cos\phi\cos\theta \end{Bmatrix} \tag{12}
$$

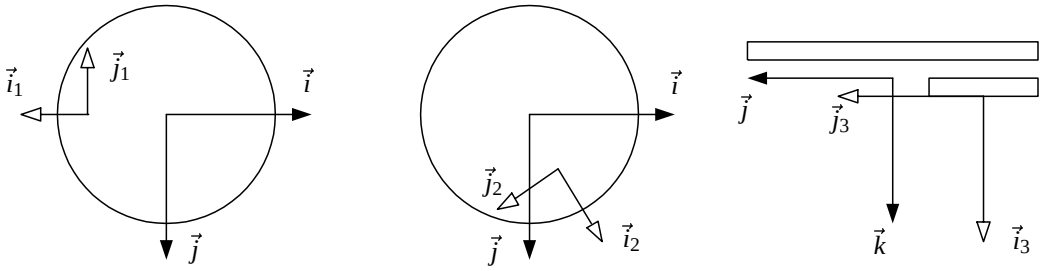

Figure 15: Coordinate Transformations

Now, equation (8) can be written as

$$
\begin{aligned}
0 &= [\tilde{K}]_S \{mg\,\vec{r}_S\}_S + [\underline{\underline{\mathbf{I}}}]_S \left\{ {}^I\dot{\vec{\omega}}^S \right\}_S + [{}^I\tilde{\omega}^S]_S [\underline{\underline{\mathbf{I}}}]_S \{{}^I\vec{\omega}^S\}_S \\
&\quad + \sum_{i=1}^{3} \left(T_{w_i S} \begin{Bmatrix} I_{11}^{w_i}\dot{\omega}_i \\ 0 \\ 0 \end{Bmatrix} + \{{}^I\vec{\omega}^S\}_S T_{w_i S} \begin{Bmatrix} I_{11}^{w_i}\omega_i \\ 0 \\ 0 \end{Bmatrix} \right) \\
&= [A]\{x\} - \{T\}
\end{aligned} \tag{13}
$$

where $[A]$, $\{x\}$ and $\{T\}$ are

$$
[A] = \begin{bmatrix} \dot{p} & \dot{q}-pr & \dot{r}+pq & -qr & q^2-r^2 & qr & \\ pr & \dot{d}+qr & r^2-p^2 & \dot{q} & \dot{r}-pq & -pr & [\tilde{K}]_S \\ -pq & p^2-q^2 & \dot{p}-qr & pq & \dot{q}+pr & \dot{r} & \end{bmatrix}
$$

$$
\{x\} = \begin{bmatrix} I_{11} & I_{12} & I_{13} & I_{22} & I_{23} & I_{33} & mg\,r_{S_x} & mg\,r_{S_y} & mg\,r_{S_z} \end{bmatrix}^T \tag{14}
$$

$$
\{T\} = -\begin{Bmatrix} -I_{11}^{w_1}\dot{\omega}_1 + \frac{1}{2}I_{11}^{w_2}\dot{\omega}_2 \\ \frac{\sqrt{3}}{2}I_{11}^{w_2}\dot{\omega}_2 \\ I_{11}^{w_3}\dot{\omega}_3 \end{Bmatrix} - \begin{bmatrix} 0 & -r & q \\ r & 0 & -p \\ -q & p & 0 \end{bmatrix} \begin{Bmatrix} -I_{11}^{w_1}\omega_1 + \frac{1}{2}I_{11}^{w_2}\omega_2 \\ \frac{\sqrt{3}}{2}I_{11}^{w_2}\omega_2 \\ I_{11}^{w_3}\omega_3 \end{Bmatrix}
$$

Let $[A_i]$ and $\{T_i\}$ be values of $[A]$ and $\{T\}$ at i^{th} time step. Define $[\tilde{A}]$ and $\{\tilde{T}\}$ as

$$
[\tilde{A}] = \begin{bmatrix} [A_1] \\ [A_2] \\ \cdots \\ [A_n] \end{bmatrix} \quad , \quad \{\tilde{T}\} = \begin{Bmatrix} \{T_1\} \\ \{T_2\} \\ \cdots \\ \{T_n\} \end{Bmatrix} \tag{15}
$$

Finally, the least square estimation of $\{I\}$ that minimizes $||[\tilde{A}]\{I\} - \{\tilde{T}_w\}||$ is given by

$$
\{\tilde{I}\} = [\tilde{A}]^{\dagger}\{\tilde{T}\} \tag{16}
$$

where $[\tilde{A}]^{\dagger}$ is generalized inverse of $[\tilde{A}]$.

To verify the regression equation and examine the numerical error from the matrix inversion, the previous inertia estimation scheme was tested using simulation data. A simple angular velocity stabilizer is used for the simulation. As is shown in Fig. 16, the error decreases as the simulation time step decreases. Thus we can conclude that the numerical error resulting from the matrix inversion is negligible.

Experimental Results

The moments of inertia of the wheels were calculated both from the AutoCAD model and the experimental approach outlined previously. Since the geometric complexity of the wheel is simple, it is assumed that the inertia values of the wheels from the CAD model are accurate. These values are given below

$$
I_{11}^{w_1} = I_{11}^{w_2} = I_{11}^{w_3} = 1.792 \times 10^{-3} \quad (\text{kg m}^2)
$$

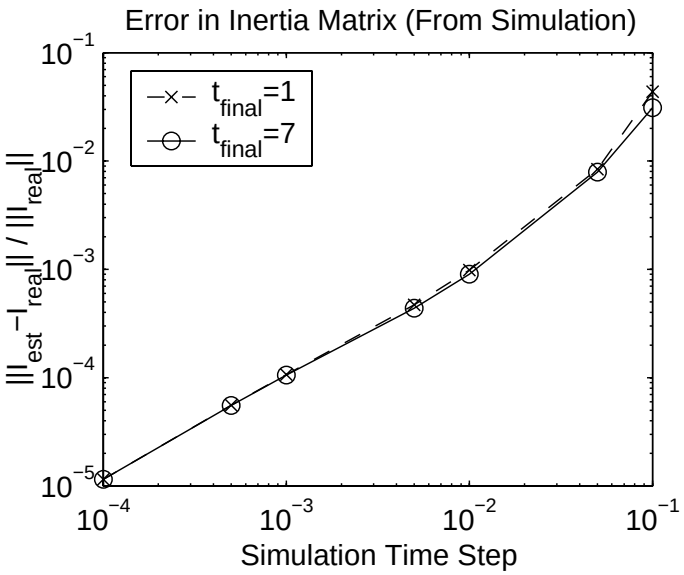

Figure 16: Verification of estimation equations by simulation

The following results are the averaged inertia matrix and the vector $mg\vec{r}_s$ from a series of ten experiments. Each experiment was performed for about 50∼80 seconds. For comparison, the inertia matrix calculated from the geometry in AutoCAD is also provided. For convenience, during the experiment the mass center was moved below the bearing center ($+z$) to make the platform stable, by adjusting a vertical counterweight. The counterweight can be moved up to make the platform neutrally stable for other experiments later. In this case, the inertia can be adjusted using the parallel axis theorem.[21]

Identified Inertia Matrix			mgr	AutoCAD		
1.1667	0.0107	-0.0185	0.0101	1.027	0.000	0.000
0.0107	1.1671	0.0159	0.0323	0.000	1.034	0.000
-0.0185	0.0159	2.1291	0.7630	0.000	0.000	1.869

The results of the experiments show remarkable consistency. The standard deviations are $\sigma(I_{xx}) = 0.0075$, $\sigma(I_{yy}) = 0.0091$, $\sigma(I_{zz}) = 0.0022$, $\sigma(I_{xy}) = 0.0049$, $\sigma(I_{xz}) = 0.0028$, $\sigma(I_{yz}) = 0.0060$, $\sigma(mgr_x) = 0.0011$, $\sigma(mgr_y) = 0.0019$ and $\sigma(mgr_z) = 0.0160$. Note that because of some components such as wires and some counter weights that are not modelled, the experimental values are somewhat larger than those found with the AutoCAD model.

RESULTS FROM AN LQR CONTROLLER IMPLEMENTATION

In this section we present some preliminary experimental results for a simple stabilizing controller. Assuming small Eulerian angles ϕ, θ one obtains that $\dot{\phi} \approx p$, $\dot{\theta} \approx q$ and $\dot{\psi} \approx r$, where p, q and r are the angular velocity components of platform expressed in a body-fixed frame. Assuming in addition that p, q and r are also small, the equations of motion (3) and (8) can be linearized about the origin. The resulting system can be written in the standard form

(18) $$\dot{x} = Ax + Bu$$

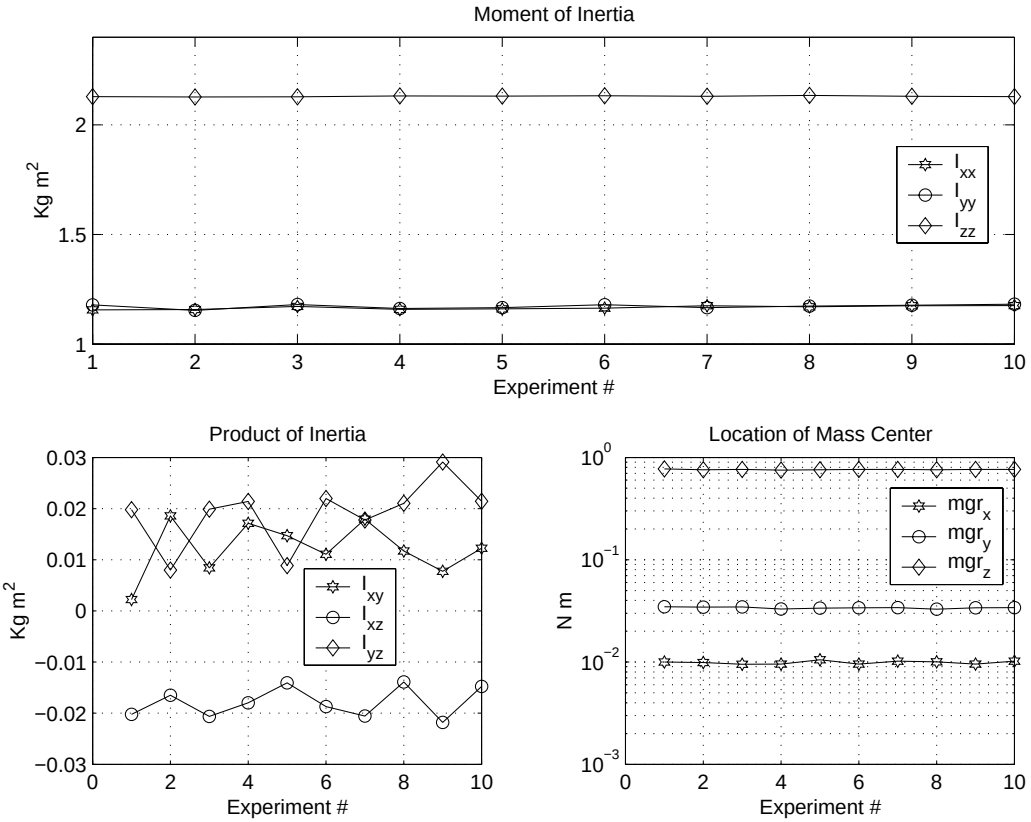

Figure 17: Results of the inertia estimation for a series of ten experiments

where $x = [\phi,\ p,\ \theta,\ q,\ \psi,\ r]^T$, and

$$A = \begin{bmatrix} 0 & 1 & 0 & 0 & 0 & 0 \\ 0 & 0 & 0 & 0 & 0 & 0 \\ 0 & 0 & 0 & 1 & 0 & 0 \\ 0 & 0 & 0 & 0 & 0 & 0 \\ 0 & 0 & 0 & 0 & 0 & 1 \\ 0 & 0 & 0 & 0 & 0 & 0 \end{bmatrix}, \qquad B = \begin{bmatrix} 0 & 1 & 0 \\ -(1/I_1) & 1/(2I_2) & 0 \\ 0 & 0 & 0 \\ 0 & \sqrt{3}/(2I_2) & 0 \\ 0 & 0 & 0 \\ 0 & 0 & 1/I_3 \end{bmatrix} \tag{19}$$

The control input is $u = [T_1,\ T_2,\ T_3]^T$ where T_i, $i = 1,2,3$ is the torque on the ith wheel.

An LQR controller that minimizes a quadratic cost of the form

$$J = \int_0^\infty \{x^T Q x + u^T R u\}\,\mathrm{d}t \tag{20}$$

where $Q \geq 0$ and $R > 0$ and stabilizes ϕ, θ, ψ, p, q and r can be designed using standard methods.[22] Using $Q = I_6$ and $R = I_3$ the state-feedback control $u = Kx$ with

$$K = \begin{bmatrix} -0.9659 & -1.6734 & 0.2588 & 0.6188 & 0 & 0 \\ 0.2588 & 0.3008 & 0.9659 & 1.7586 & 0 & 0 \\ 0 & 0 & 0 & 0 & 1 & 3.7197 \end{bmatrix} \tag{21}$$

The experimental results for two different initial conditions of such an LQR controller are shown in Fig. 18.

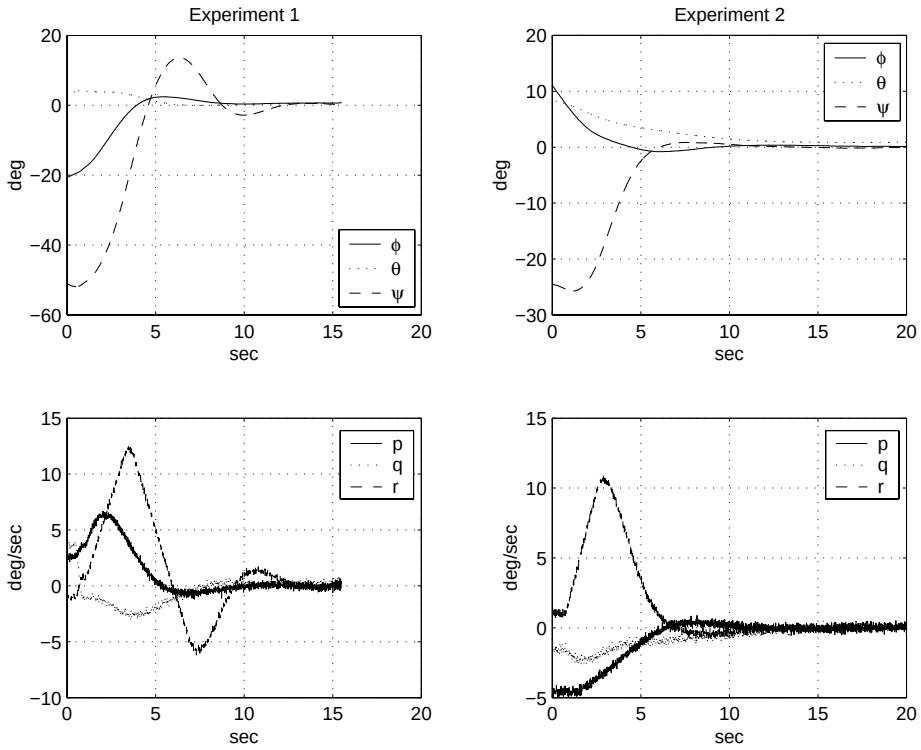

Figure 18: Experimental results of LQR controller.

CONCLUSIONS

A spacecraft simulator facility has been designed and constructed at the School of Aerospace Engineering at the Georgia Institute of Technology. The simulator is to be used primarily for research in advanced nonlinear attitude control law design and implementation. Secondarily will be used to educate graduate and undergraduate students in spacecraft attitude dynamics and control. During the construction of the simulator several issues were encountered. Such issues included choice of motors, the sizing of the wheels, sensor range and resolution, etc. Identification of motor dynamics and friction and motor damping estimation was deemed necessary to better estimate the motor characteristics. Special purpose software was written to implement the control laws and schedule the several hardware tasks. The mass and moments of inertia of the spacecraft simulator platform were estimated using a least-squares approach by commanding known torques and observing the angular acceleration response. The results from several experiments showed good consistency. These results corroborated the mass and inertia values obtained with an AutoCAD model. After careful balancing the platform, an LQR controller was designed based on a linearized model of the system and was implemented on the simulator. The initial experimental results were consistent with those obtained via numerical simulations.

Acknowledgement: The work in this paper was supported in part by AFSOR Award No: F49620-00-1-0374 and NSF Award No: CMS/REU-9996120.

REFERENCES

[1] K. Lau, M. Colavita, G. Blackwood, Linfield R., M. Shao, and D. Gallagher. The new millennium formation flying optical interferometer. In *AIAA GNC Conference*, 650–656, 1997. Paper AIAA 97-3820.

[2] R. L. Grogan and R. A. Laskin. On multidisciplinary modeling of the space interferometry mission. In *American Control Conference*, pages 1558–1562, 1998. Philadelphia, PA.

[3] A. Robertson, T. Corazzini, and J. How. Formation sensing and control technologies for a separated spacecraft interferometer. In *American Control Conference*, pages 1574–1579, 1998. Philadelphia, PA.

[4] P. Wang, F. Y. Hadaegh, and K. Lau. Synchronized formation rotation and attitude control of multiple free-flying spacecraft. *Journal of Guidance, Control, and Dynamics*, 22(1):28–35, 1999.

[5] C. Sabol, R. Burns, and McLaughlin. Satellite formation flyng design and evolution. *Journal of Guidance, Control, and Dynamics*, 38(2):270–278, 2001.

[6] R. W. Beard, J. Lawton, and F. Y. Hadaegh. A feeback architecture for formation control. In *American Control Conference*, pages 4087–4091, 2000. Chicago, IL.

[7] M. de Queiroz, V. Kapila, and Q. Yan. Adaptive nonlinear control of multiple spacecraft formation flying. *Journal of Guidance, Control, and Dynamics*, 23(3):385–390, 2000.

[8] D. J. Jezewski, J. P. Brazzel Jr., E. E. Prust, B. G. Brown, T. A. Mulder, and D. B. Wissinger. A survey of rendezvous trajectory planning. In *AAS/AIAA Astrodynamics Conference, Durango, CO, August 19-22, 1991*, pages 1373–1396. San Diego, CA, Univelt, Inc., 1991. AAS paper 91-505.

[9] T. A. Mulder. Autonomous rendezvous trajectory planning. In *Proceedings of the 2nd AAS/AIAA Spaceflight Mechanics Conference, Colorado Springs, CO., Feburary 24-26, 1992*, pages 709–719. San Diego, CA, Univelt, Inc., 1992. AAS Paper 92-104.

[10] M. R. Helton. Refurbishable satellites for low cost communications systems. *Space Communication and Broadcasting*, 6:379–385, 1989.

[11] D. Manouchehri and A. J. Mauceri. Automated resuply of consumables: Enhancement of space commercialization opportunities. In *The 5th Annual Workshop on Space Operations Applications and Research (SOAR 1991)*, volume 1, pages 407–411, 1991. In NASA. Johnson Space Center.

[12] A. Das, Berg J. L., G. A. Norris, D. F. Cossey, T. J. Strange III, and Schlaegel. W. T. ASTREX - a unique test bed for CSI research. In *Proceedings of the 29th IEEE Conference on Decision and Control*, pages 2018–2023, 5-7 Dec. 1990. Honolulu, HI.

[13] B. N. Agrawal and R. E. Rasmussen. Air bearing based satellite attitude dynamics simulator for control software research and development. In *SPIE AeroSense, Modeling, Simulation, and Visualization Conference*, April 17, 2001. Orlando, FL.

[14] J. A. Mangus, C. Passerello, and C VanKarsen. Estimating rigid body properties from force reaction measurements. In *Preceedings of the 11th International Modal Analysis Conference*, pages 469–472, February 1-4 1993. Kissimmee, FL.

[15] M. A. Stebbins and D. L. Brown. Rigid body inertia property estimation using a six-axis load cell. In *Preceedings of the 16th International Modal Analysis Conference*, pages 900–906, February 2-5 1998. Santa Barbara, CA.

[16] S Tanygin and T Williams. Mass property estimation using coasting meneuver. *Journal of Guidance, Control and Dynamics*, 20:625–632, 1997.

[17] E. V. Bergmann, B. K. Walker, and D. R. Levy. Mass property estimation for control of asymmetrical satellites. *Journal of Guidance, Control, and Dynamics*, 10:483–491, 1987.

[18] R. F. Richfield, B. K. Walker, and E. V. Bergmann. Input selection for a second order mass property estimator. *Journal of Guidance, Control, and Dynamics*, 11:207–212, 1988.

[19] J. Ahmed, V. T. Coppola, and D.S. Bernstein. Adaptive asymptotic tracking of spacecraft attitude motion with inertia matrix identification. *Journal of Guidance, Control, and Dynamics*, 21:684–691, 1998.

[20] R. H. Bishop, S. J. Paynter, and J. W. Sunkel. Adaptive control of space station with control moment gyros. *IEEE Control Systems Magazine*, 12:23–28, 1992.

[21] P. C. Hughes. *Spacecraft Attitude Dynamics*. John Wiley & Sons, New York, 1986.

[22] R. F. Stengel. *Optimal Control and Estimation*. Dover, New York, 1994.